Probabilistic hazard analysis for tsunamis generated by subaqueous volcanic explosions in the Campi Flegrei caldera, Italy

Raphael Paris, M. Ulvrova, J. Selva, B. Brizuela, A. Costa, A. Grezio, S. Lorito, R. Tonini

Probabilistic hazard analysis for tsunamis generated by subaqueous volcanic explosions in the Campi Flegrei caldera, Italy

R. Paris[1], M. Ulvrova[2], J. Selva[3], B. Brizuela[4], A. Costa[3], A. Grezio[3], S. Lorito[4], R. Tonini[4]

[1] Université Clermont Auvergne, CNRS, IRD, OPGC, Laboratoire Magmas et Volcans, F-63000 Clermont-Ferrand, France.

[2] Institute of Geophysics, Department of Earth Sciences, ETH Zürich, Zürich, Switzerland

[3] Istituto Nazionale di Geofisica e Vulcanologia, Sezione di Bologna, Bologna, Italy

[4] Istituto Nazionale di Geofisica e Vulcanologia, Sezione di Roma 1, Roma, Italy

* Corresponding author at: Université Clermont Auvergne, CNRS, IRD, OPGC, Laboratoire Magmas et Volcans, F-63000 Clermont-Ferrand, France.Tel. +33 473346717. E-mail. Raphael.Paris@uca.fr

Abstract

A probabilistic hazard analysis of tsunami generated by subaqueous volcanic explosion is applied to the Campi Flegrei caldera (Campania, Italy). An event tree is developed to quantify the tsunami hazard due to the submarine explosions by: *i)* defining potential size classes of explosion magnitude on the basis of past volcanic activity in the Campi Flegrei caldera and sites in the underwater part of the caldera; *ii)* simulating the generation and propagation of the consequent tsunami waves able to reach the coasts of the Campania region for all combinations of tsunami-generating vents and sizes; and *iii)* quantifying the tsunami probability and relative uncertainty, conditional upon the occurrence of an underwater eruption at Campi Flegrei. Tsunami hazard generated by subaqueous volcanic explosions is considered crucial because of its potential high impact on the densely populated coastal areas of the Pozzuoli Bay and Gulf of Naples even if the probability for eruptions in the submarine part of the caldera is certainly low. The tsunami hazard analysis is presented using conditional hazard curves and maps, that is calculating the probability (and relative uncertainties) of exceeding given tsunami intensity thresholds (wave amplitudes at the coast), given the occurrence of a subaqueous eruption. The results indicate that a significant tsunami hazard exists in many areas of the Bay of Naples.

Keywords: volcanic tsunami, submarine volcanic explosions, caldera volcano, Campi Flegrei caldera

1. Introduction

Tsunamis generated by eruptive and gravitational processes on the flanks of volcanic edifices are quite infrequent (about 5% of all recorded tsunamis: Latter, 1981), but they represent the third cause of fatalities due to volcanism, with four tsunamigenic eruptions being ranked in the twenty deadliest volcanic disasters (e.g. Auker et al., 2013). Tsunami hazards related to subaqueous eruptions are particularly challenging to evaluate and forecast, due to a lack of geological, observational and instrumental data, in particular in densely populated regions such as the Campi Flegrei caldera in Italy (Fig. 1).

Different tsunami source mechanisms can be involved during a subaqueous eruption: pyroclastic flows, debris flows, caldera collapses and explosions (Paris, 2015). Tsunami generation by subaqueous volcanic explosions is controlled by a range of physical parameters including water depth, size of eruptive vent, energy and depth of explosion, and complex magma-water interactions which determine the explosion itself (Le Méhauté, 1971; Kokelaar, 1986; Wohletz, 1986; Mirchina & Pelinovsky, 1988; Duffy, 1992; Le Méhauté & Wang, 1996; Kedrinskii, 2005; Egorov, 2007; Morrissey et al., 2010). The explosion forms an initial crater-like cavity at the water surface (Fig. 2a), with a cylindrical bore that expands radially to form the leading wave, followed by a wave trough. Initial surface displacement of the water surface (i.e. maximum height of the bore) can be empirically estimated directly as a function of explosion energy at a given water depth and size of the formed eruptive vent (Le Méhauté, 1971; Sato & Taniguchi, 1997; Goto et al., 2001). The initial downward displacement of the water column (i.e. the cavity) is followed by an upward displacement, thus forming a steep cone of water in the centre. This cone then collapses and turns to a second cylindrical bore, as demonstrated by experimental explosions and numerical simulations (e.g. Le Méhauté & Wang, 1996; Kedrinskii, 2005; Torsvik et al., 2010; Ulvrova et al., 2014 & 2016; Paris & Ulvrova, 2019).

Different methods of Probabilistic Tsunami Hazard Analyses (PTHA) have been developed during the two last decades (Grezio et al., 2017). PTHA provides the likelihood of a given parameter of the tsunami (e.g. wave height at the coast, flow velocity, flow depth, runup height, or inundation distance) being exceeded at a particular location within a given period of time. PTHA can combine geological, historical and instrumental data both of tsunamis (e.g. sedimentary deposits, catalogues and historical accounts, tide-gauge records or pressure sensor time-series), and of tsunami sources (source parameters, such as fault and seismicity catalogue for earthquake sources), using statistical techniques and numerical simulations. Due to the low relative frequency of tsunamis, concurring with the lack of repeated tsunami run-up data spanning a long enough time period at a given location, the common practice is to propose numerous different tsunami source scenarios with their associated probability (Geist and Lynett, 2014). These scenarios are assumed to be a complete representation of the expected natural variability (Selva et al., 2016). However, PTHA methods for landslide and volcanic sources of tsunamis are far less established compared to the earthquake sources (Grezio et al., 2017). Here, we produce a first attempt of considering volcanic sources. We focus on conditional PTHA, that is, conditional upon the occurrence of a volcanic phenomenon potentially generating a tsunami (i.e. submarine eruptions). The quantification of long-term conditional hazard is common in volcanic hazard studies, since it allows for planning evacuation in case of eruption (e.g. update of the National Emergency Plan for Campi Flegrei, 2016: http://www.protezionecivile.gov.it/en/media-communication/dossier/detail/-/asset_publisher/default/content/aggiornamento-del-piano-nazionale-di-emergenza-per-i-campi-flegrei), as well as it provides reference simulations for short-term hazard quantifications (e.g., Selva et al., 2014). Its extension to absolute PTHA may be obtained by multiplying conditional hazard by the probability of occurrence of volcanic eruption. With more than 20 eruptions in the last 5 ka (e.g. 25 eruptions listed by Orsi et al., 2009), eruptions at Campi Flegrei have a mean annual rate on the order of 10^{-3} per year. However, we did not attempt here the estimation of any temporal component of the hazard, which is not trivial being volcanic eruptive sequences clearly not stationary in time (Bevilacqua et al., 2016).

In this study, we consider different scenarios of tsunamis generated by explosions in the offshore part of the Campi Flegrei caldera (Campania, Italy) and their effects on the coasts of the Pozzuoli Bay, the islands of Ischia and Capri, and the Gulf of Naples (Figs. 1 and 2a). These scenarios include different potential sizes and vent positions within the Campi Flegrei

caldera. They are then combined according to their probability of occurrence, quantifying the consequent hazard in terms of conditional PTHA. The nested caldera of Campi Flegrei is a complex partly submerged volcanic structure created mainly by multiple caldera forming events: the 39 ka Campanian Ignimbrite, the 29 ka Masseria del Monte Tuff, and the 12 ka Neapolitan Yellow Tuff (e.g. Deino et al., 2004; Marti et al., 2016; Albert et al., 2019). During the last 12 ka, periods of high-frequency volcanism (mean intervals of 50-70 years) were separated by periods of quiescence lasting from 1 to 3.5 ka (Di Vito et al., 1999). While the onshore eruptive history of the caldera is well documented, past volcanic activity offshore and the probability for future eruptions in the submarine part of the caldera (Pozzuoli Bay) have been rarely discussed (Tonini et al., 2015; Selva et al. 2012a). Recent seismic and magnetic surveys allowed the structural and magmatic evolution of the submerged southern half of the caldera to be reconstructed (Aiello et al., 2012; Steinmann et al., 2018). The explosivity of coastal-to-submarine eruptions such as Nisida Bank (~10 ka), Nisida Island (~4 ka), and Capo Miseno (~3.7 ka) was recently reassessed to at least VEI 3 (Steinmann et al., 2018). Highly permeable ring-faults along the southern rim of the caldera are prone to magma ascent (Steinmann et al., 2018) and represent potential sites for future eruptions (Selva et al., 2012a). Moreover, structural and geophysical data indicate the presence of several major faults in the submerged part of the caldera, representing potential weakness areas in which eruption may be favoured (Selva et al., 2012a). Along these structures, the last eruption of Campi Flegrei (Monte Nuovo, A.D. 1538) occurred starting at sea (Guidoboni and Ciuccarelli, 2011; Di Vito et al. 2016).

2. Methods

The methodology presented in this paper is based on the development of an event tree (Newhall and Hobblit, 2002) for quantifying the tsunami hazard due to submarine explosions. This method is based on 3 major steps: (1) the event tree was set by identifying 17 potential vent areas in the underwater part of the Campi Flegrei caldera and 4 size classes of eruptive events (three of which tsunami-generating explosive eruptions), allowing the definition of 17×3 representative tsunami-generating scenarios; (2) all the representative scenarios were simulated, generating and propagating the consequent tsunami waves able to reach the coasts of the Campania region; (3) the conditional probability of each representative scenario given the occurrence of one eruption at sea was estimated, and combined with the corresponding

simulated tsunami scenarios, to produce the final conditional PTHA in the event-tree framework.

2.1. Setting the event tree to represent vent and size variability of eruptions

We considered here only those explosions deemed capable to generate tsunamis, i.e. eruptions occurring at sea with depth greater than 10 m. The adopted event tree for the Campi Flegrei caldera (Fig. 3) is the modified Bayesian Event Tree for Volcanic Hazard (BET_VH) by Selva et al. (2010). Nodes 1-2-3 can be neglected, since probabilities are conditioned upon the occurrence of an eruption. Then, the residual event tree is composed only by 4 levels, which are relative to vent position, eruption size, and tsunami generation and intensity (nodes 4, 5, and 6-7-8, following Marzocchi et al. 2010).

At node 4 (vent position on Fig. 3), we reduced the original discretization from Selva et al. (2012a) in order to decrease the computational cost of the subsequent tsunami simulations, adopting a regular grid with cell size of 1500×1500 m. Limiting only to the areas with not null conditional probability and water depth $D > 10$ m, we selected 17 equally spaced cells in the Pozzuoli Bay (Fig. 2b) as potential eruptive sites. Note that the explosion depth (d) used in the simulations is similar to water depth (D) and ranges between 23 and 111 m (Table 1).

At node 5, we adopted the four size classes for eruptions proposed by Orsi et al. (2009), in line also with most of subsequent probabilistic volcanic hazard quantifications at Campi Flegrei (Costa et al., 2009; Selva et al. 2010, 2014, 2018; Tonini et al. 2015, Sandri et al., 2016). Only 3 out of the size classes are relative to explosive eruptions. To characterize these explosive classes in terms of tsunami-generation potential, we estimated the corresponding crater dimensions using an analysis of the past activity in the caldera in three different epochs of volcanic activity (Orsi et al., 2009). In epoch 1 (15-9.5 ka Before Present) 34 explosive eruptions occurred, in epoch 2 (8.6-8.2 ka BP) 6 explosive eruptions and in epoch 3 (4.8-3.8 ka BP) 22 explosive and 3 effusive eruptions (di Vito et al., 1999; Orsi et al., 2009) (Fig. 2c and 2d). On the basis of the correspondent crater characteristics, the explosive eruptions are grouped in three size classes in terms of vent radius, corresponding to different explosive energies. Thus, we selected 3 radius values (200, 650, and 900 m) as representative of the three eruption classes. We assume that both submerged and emerged areas of the Campi Flegrei undergo to similar explosive processes in the caldera.

157 At node 6, we considered only tsunamis generated by explosive eruptions. Of course, other
158 volcanic processes, such as flank collapses or pyroclastic density currents entering the sea,
159 may generate tsunami waves

160 At node 7-8 (Fig. 3), we adopted a "representative scenario" approach (Selva et al. 2010). In
161 this approach, each of the combinations of the 17 cells and 3 size classes is represented by a
162 single scenario with representative parameters (cell centre and representative radius), instead
163 of modelling the variability of both vent positions in each cell and crater sizes in each size
164 class (Sandri et al. 2016). In this way, the latter variability (intra-class) is assumed negligible
165 with respect to the inter-class variability (the one between the different representative vent
166 and size classes). Sandri et al. (2016) demonstrated that this approach is reasonable as first
167 order approximation for tephra fallout in the Probabilistic Volcanic Hazard Analysis (PVHA)
168 at both Somma-Vesuvius and Campi Flegrei, by quantifying the bias induced by adopting one
169 single representative scenario instead of sampling its natural variability. Given that we
170 adopted the same discretization for size classes, we assume that this can be extended to the
171 tsunami hazard. As a consequence, we defined 17×3 representative scenarios of explosions
172 with vent positioned in the geometrical centre of each of the 17 cells, and representative
173 radius of 200, 650, and 900 m for the three explosive classes.

174

175 *2.2 Numerical simulations of explosion and tsunami*

176 All the combinations of representative 17 vent locations and 3 vent sizes should be considered
177 as potential source for tsunamis. The energy of the explosion is estimated following the
178 empirical relationship given by Sato and Taniguchi (1997):

179 $E = 3.56 \times 10^7 R^3$ (Eq. 1)

180 where E is the explosion energy in Joules and R the radius of the eruptive vent in meters.
181 Following the method proposed by Torsvik et al. (2010) and Ulvrova et al. (2014, 2016), and
182 using the empirical formula of Le Méhauté and Wang (1996), the initial surface displacement
183 generated by the explosion is a parabolic cavity with a vertical steep water rim. The size of
184 the water cavity (R_c, in meters) is then estimated based on explosion energy using relationship
185 (Le Méhauté and Wang, 1996):

186 $R_c = 0.0361\ E^{0.25}$ (Eq. 2)

The initial maximum vertical water surface displacement η_0 of the cavity rim is also a function of explosion energy at a given depth following:

$$\eta_0 = c\, E^{0.24} \qquad \text{(Eq. 3)}$$

based on the empirical formula of Le Méhauté and Wang (1996, with η_0 is in meters, and c is an empirical dimensional constant. According to the explosion yield and water depth, two cases are distinguished (Le Méhauté and Wang, 1996): (1) $c = 0.0143$ if $6.15\times10^{-4} < d/E^{1/3} < 1.85\times10^{-2}$ (where d is the depth of explosion in metres); or (2) $c = 0.0291$ if $d/E^{1/3} < 6.15\times10^{-4}$. Values of explosion energy (E) and corresponding initial surface displacement (η_0) of the 51 simulated scenarios are listed in Table 1.

All numerical simulations were performed using FUNWAVE-TVD code solving for the fully non-linear Boussinesq-type wave equations in spherical coordinates (Kirby et al., 1998; Shi et al., 2012; Tehranirad et al., 2013). Boussinesq model includes the effects of amplitude non-linearity and frequency dispersion in the case of intermediate-to-deep water waves (up to wavelengths equivalent to water depth) although we neglect the effect of bottom friction. The third-order Runge-Kutta method is used to advance the model in time. An adaptive time step is chosen following the Courant-Friedrichs-Lewy criterion. To ensure the stability of the scheme, we set the Courant number to 0.5 and keep it constant for all simulations. Fourth-order spatial discretization is employed. We exploit only the maximum amplitude of the incoming waves at the shoreline and neglect the inundation phase. We run the simulations for 25 minutes of the model time. In order to prevent reflections from the end-walls at the open sea, we impose a 3 km wide sponge layer at the limit of the computational domain.

The spherical grid has a resolution of 39 m ×50 m (893×1595 grid nodes) in the longitudinal and latitudinal directions, respectively, covering about an area of 3000 km^2 between Ischia, Capri and Naples (Fig. 1). The grid was built by integrating printed nautical charts to digital elevation (Tarquini et al., 2007) and bathymetric models (D'Argenio et al., 2004) available for the study area. Typical water depth in the Gulf of Naples and Pozzuoli Bay ranges between 50 and 200 m. Wave heights at the coast were computed at >200 virtual tide gauge stations from Pozzuoli to Amalfi, including Ischia and Capri Islands.

2.3. Probabilistic hazard analysis

The probability at nodes 4 and 5 of the Event Tree are retrieved from literature. In particular, for node 4, we adopted the probability proposed by Selva et al. (2012a), cumulating the distribution parameters of the undersea (depth > 10 m) cells closer to our 17 selected vent positions. This probability distribution is not uniform, being eruptions in the centre of the gulf more probable due to the presence of main NE-SW trending fault system. At node 5, we adopted the distribution parameters of Orsi et al. (2009), as updated in Selva et al. (2018), with a decreasing probability for increasing explosion size.

At node 6, we assume that effusive eruptions certainly do not produce tsunamis (conditional probability equal to 0 and no epistemic uncertainty), while explosive eruptions certainly produce tsunamis (conditional probability equal to 1).

At nodes 7-8, as tsunami intensity measure we selected the maximum wave amplitude (*Hmax*) recorded at the coast (at a water depth of 1 m). Hazard curves were built at 421 target points along the coast, from Cuma to Positano. To account for the rather rough discretization of the aleatory distribution on source space (based on a broad grid for the vents and only 3 potential sizes), as well as for the intrinsic uncertainty in the generation and propagation of the tsunami, we introduced some level of uncertainty to the simulation results (Glimsdal et al., 2019). We assumed that each scenario is associated to a conditional hazard curve (conditional upon a scenario in that vent area and that size class) described by a log-normal distribution (see Davies et al. 2017, and references therein). The parameters of the distribution (μ and σ, mean and standard deviation of the logarithmic values, respectively) were set based on simulation results. Specifically, we set μ as the average value of the log(*Hmax*), while a rather large variance is assumed by setting $\sigma = 1$ (slightly larger than the one adopted for earthquake generated tsunamis in Davies et al. 2017). Given the first order approximation made by defining in this way the log-normal distribution, we set to the obtained conditional hazard curves the maximum allowed epistemic uncertainty (equivalent sample size equal to 1).

3. Results

3.1. Tsunami wave heights at the coast

246 The three scenarios of explosions with vent radius, R, of 200, 650, and 900 m, correspond to
247 explosion energies, E, of 2.9×10^{14}, 9.8×10^{15}, and 2.6×10^{16} J (Table 1). Following Eq. (3),
248 these explosions create an initial surface displacement of the water surface, η_0, of 85, 200, and
249 250 m, respectively (Table 1). Tsunami waves generated by the explosion propagate radially
250 away from the explosion centre, all over the computational area, with a significant influence
251 of the bathymetry (e.g. higher wave heights due to shallow banks around the Dohrn and
252 Magnaghi canyons in Fig. 4) and coastal morphology (e.g. effects of wave refraction around
253 the islands and capes in Fig. 4).

254 The highest tsunami impact is recorded on the coasts of the Pozzuoli Bay that are in the
255 imminent vicinity of the explosion centres. Maximum wave heights at the coast exceed 3 m
256 only in the Pozzuoli Bay and the eastern coast of Procida Island. Wave heights decrease by a
257 factor of 10 from the explosion site to the Gulf of Naples (note logarithmic scale of wave
258 heights on Fig. 4), where all sites record waves lower than 1.5 m for the scenarios with R =
259 900 m and lower than 0.5 m for the scenarios with R = 650 m. As a result of wave refraction,
260 secondary peaks of wave heights are observed on the western coast of the Sorrento Peninsula
261 and eastern coast of Capri Island (i.e. at distances between 80 and 110 km on Fig. 5).

262 For a vent radius of 900 m (η_0 = 250 m), wave heights higher than 10 m are restricted to the
263 coasts of the Pozzuoli Bay (Figs. 4 and 5). Lowering vent radius to 650 m (η_0 = 200 m)
264 reduces wave heights in the bay by a factor of 1.5 to 2 (Fig. 5). Wave height profiles recorded
265 at different tide gauge stations show that the scenarios with vent radius of 900 m generate
266 waves twice as high as the one with vent radius of 650 m (Fig. 6). Apart from this difference,
267 the two cases display the same wave patterns. Explosions corresponding to a vent radius of
268 200 m (η_0 = 85 m) generate waves lower than 1 m high, even on the coasts of the Pozzuoli
269 Bay (Figs. 5 and 6), except at vent sites #16 and #17 (Fig. 2b) which are located near the
270 coast. In this case, waves locally reach amplitudes up to 2 meters (Fig. 5).

271 The propagation of the tsunami in the entire Gulf of Naples takes approximately 15 minutes.
272 Waves reach Pozzuoli in 2 minutes, Procida in 4 minutes, Naples in 7 minutes, Capri in 9
273 minutes, and Castellamare di Stabia in 13 minutes (Fig. 6). The positive leading wave (peak)
274 is the highest one, except for the stations located on the opposite side of the Gulf of Naples
275 (e.g. Castellamare di Stabia, Capri). In the proximal field, the leading wave represents the
276 short-period component of the wave spectrum (e.g. Pozzuoli, Procida, and Naples). As the
277 distance from the explosion increases, the arrival of longer-period waves might predate the

short-period waves because they travel faster in the Gulf of Naples. This is a direct effect of frequency dispersion. At Castellamare di Stabia, the 0.7 m-high leading wave is followed by higher waves progressively reaching a maximum height of 1.5 m (Fig. 6).

3.2. Probabilistic conditional hazard curves and maps

We produced tsunami hazard curves that are conditional to subaqueous eruptions, since only eruptions with vent at sea are considered. Following Selva et al. (2018), the probability to have a vent at sea (depth $D > 10$ m) given an eruption is approximately 0.11 (mean of the epistemic uncertainty). Given one eruption, the probability of being an explosive one is about 0.89 (mean of the epistemic uncertainty). Therefore, the probability to have a tsunami-generating eruption conditional upon the occurrence of an eruption of any size in any vent at Campi Flegrei is approximately equal to $0.11 \times 0.89 = 0.10$ (again, mean of the epistemic uncertainty).

The main results of the PTHA are presented as conditional hazard curves for each of the 421 target points along the coast, conditional upon the occurrence of an eruption at sea, and their respective epistemic uncertainty. In Figure 7, we reported some example of conditional hazard curves and hazard maps (mean of the epistemic uncertainty) corresponding to an exceedance probability value of 0.05, either relative to one specific eruption size or integrating all potential sizes. The value of 0.05 is chosen as a reference value as it is the same adopted for the real planning in this area (e.g. update of the National Emergency Plan for Campi Flegrei, 2016). More specifically, in the top three panels we reported the hazard maps conditional upon an explosive eruption at sea of size small (with representative radius $R = 200$ m), medium ($R = 650$ m), and large ($R = 900$ m), respectively. In the bottom panel, we combined all potential eruption sizes (including the non-tsunami-generating effusive size, in analogy with Selva et al., 2008; 2018 and Sandri et al., 2016), reporting the conditional hazard map given an eruption at sea for any size.

The results for the single eruptive classes show that the tsunami intensities may be significant in case of explosive eruption at sea, with intensities corresponding to 0.05 exceedance probability (mean of the epistemic uncertainty) always significant (> 1 m) inside the Pozzuoli bay, reaching tens of meters for medium and large explosive eruption classes (Fig. 7). In the case of medium and, even more, large explosive eruptions, significant intensities were found

also in many areas of the larger Bay of Naples, with focalization point along the Sorrento peninsula.

As observed for other hazards (e.g., tephra fallout in Sandri et al. 2016 and Selva et al. 2018), the hazard maps integrating all sizes provide results similar to the one conditioned to medium explosive eruption size, with slightly smaller intensity. Noteworthy, also integrating all potential sizes, eruptions at sea determine a significant tsunami hazard in many areas of the Bay of Naples, still with the largest potential intensities within the Pozzuoli Bay.

4. Discussion

Tsunami hazard related to subaqueous volcanic explosions in the study area, and particularly in the Pozzuoli Bay, is far from negligible, even if the probability for eruptions in the submarine part of the caldera is rather low. Considered largest scenarios of explosions (R=900 m) generate waves higher than 10 m in the Pozzuoli Bay, but lower than 1.5 m in the Gulf of Naples. Wave refraction creates local amplification (e.g. eastern coast of Capri) that is well reproduced by the numerical models. The smallest explosions considered here (R=200 m) do not represent a high hazard in terms of tsunami generation (waves < 1 m high). However, the impact of such small tsunami waves should not be neglected on such densely populated coasts. Another difficulty in terms of potential hazard mitigation actions comes from the proximity of the tsunami source. The propagation of the tsunami in the entire Gulf of Naples takes only 15 minutes. Pozzuoli is affected in less than 2 minutes.

In this work, tsunami wave behaviour at the coast (e.g. wave breaking, interaction with coastal structures) and inundation inland were not simulated, because it would require high-resolution terrain models (typically 1 m grid resolution). In the near future, such simulations could be conducted at the local scale, i.e. on areas of specific interest (e.g. harbours), using those at the larger scale as input (Lorito et al., 2015; Volpe et al., 2019).

Another limitation comes from the model of explosion itself. We considered that the size of the crater reflects the most powerful explosion at shallow depth, regardless the total number of explosions (Goto et al., 2001; Taddeucci et al., 2010). In fact, the morphology of the crater might result from multiple vertically and horizontally-migrating explosions (e.g. Valentine et al., 2012; 2015). Thus, assuming that the size of the crater corresponds to the size of the explosion might lead to an overestimation of the explosion energy in some cases.

We also assumed that the explosion occurs at the sea floor or at the rim of a pre-existing eruptive vent. However, the evolution of the vent geometry during the eruption (crater excavation, growth of the ejecta ring) and location of the explosion inside the vent might have an influence on tsunami generation. These relationships have never been tested experimentally or numerically.

Due to computational cost, we reduced exploration of aleatory variability such as vent position and its size. This limitation was compensated by introducing a rather large uncertainty into simulation results. However, given the illustrative character of this application, we did not exploit any detailed analysis to better constrain the uncertainty quantification. Temporal rates of eruptions are also difficult to constrain and, for this reason, we did not extend our results to absolute unconditional probabilities, in line with previous studies of this type (e.g. Sandri et al. 2016; Selva et al. 2018). However, we note that hazard curves conditional upon eruption may represent a direct input for decision making. Indeed, being possible short-term forecast of eruptions (e.g., Selva et al., 2012b), emergency plans are usually based on such conditional hazard estimations (e.g. update of the National Emergency Plan for Campi Flegrei, 2016). The probability of vents at sea is also poorly constrained.

Only few hazard analyses include the submerged part of Campi Flegrei as potential area for vent opening (Tonini et al., 2015). The presence of several major faults oriented NW-SE in the central part of the Pozzuoli Bay (see Orsi et al. 1994 and Selva et al. 2012a) tends to concentrate the probability of vent opening in this part of the submerged caldera. Ring-faults along the southern rim of the caldera also represent potential sites for future eruptions (Steinmann et al., 2018), but this has not been considered in this paper.

In this study, we considered only tsunami source generated by submarine volcanic explosions at Campi Flegrei. However, other sources such as pyroclastic density currents entering the sea or earthquakes and landslides should be integrated into the probabilistic analysis to avoid bias in the tsunami hazard assessment (Grezio et al., 2015). For Campi Flegrei, submarine explosions seem to be the dominating tsunami-generating volcanic process, given the topo-bathymetric configuration of the caldera and the prevalence in the past of dilute pyroclastic density currents. However, other significant sources of volcanic tsunamis are present in the Bay of Naples, including Ischia (Paparo and Tinti 2017 and reference therein) and Vesuvius (Tinti et al. 2004). The Euro-Mediterranean Tsunami Catalogue (Maramai et al., 2014) describes the sea withdrawals, sea retreats, and sea oscillations associated to volcanic

activities and reports tsunamis with intensity 2 (meaning waves lower than 1 m), mainly associated to pyroclastic density currents generated during explosive eruptions at Mt. Vesuvius.

5. Conclusion

The conditional probabilistic hazard assessment for tsunamis generated by subaqueous volcanic explosions is presented for the Campi Flegrei caldera. The probability for eruptions in the submarine part of the caldera is rather low, but scenarios of tsunamis generated by subaqueous volcanic explosions and their potentially high impact in the Pozzuoli Bay and Gulf of Naples deserve to be considered due to high population density of these coastal areas. We demonstrated that tsunamis from volcanic explosions in the Campi Flegrei caldera represent a significant source of hazard in the Pozzuoli Bay and Gulf of Naples. This is often overlooked, but should be integrated into the evaluation of natural hazards of the area. Highest hazard is found on the coasts of the Pozzuoli Bay, where incoming tsunami waves exceeding locally 10 m can be expected in case of future large explosions. Around Naples, where coasts are densely populated, the hazard is lower, but tsunamis exceeding 1 m are assessed. In this study, we considered tsunamis generated by volcanic explosions only, but other tsunamis sources such as earthquakes or landslides should be included in the future to fully evaluate the hazard in the region. Future developments could be the evaluation of a complete PTHA due to volcanic processes in the Campania region considering underwater caldera explosions, landslides, and pyroclastic density currents both from Vesuvius and Campi Flegrei eruptions.

Acknowledgements

This research was financed by the French Government Laboratory of Excellence initiative n° ANR-10-LABX-0006, the Region Auvergne, the European Regional Development Fund, and ASTARTE collaborative project FP7-ENV2013 6.4-3. M.Ulvrova has received funding from the European Union's Horizon 2020 research and innovation programme under the Marie Sktodowska-Curie grant agreement No.753755. We wish to thank G. Vilardo (Laboratory of Geomatics and Cartography, INGV-OV) for providing the topo-bathymetric data of the Neapolitan area. This is Laboratory of Excellence ClerVolc contribution n° xx.

403

404 **References**

405 Aiello, G., Marsella, E., Di Fiore, V., 2012. New seismo-stratigraphic and marine magnetic
406 data of the Gulf of Pozzuoli (Naples Bay, Tyrrhenian Sea, Italy): inferences for the
407 tectonic and magmatic events of the Phlegrean Fields volcanic complex (Campania).
408 Marine Geophysical Research 33, 97-125.

409 Albert P.G., Giaccio B., Isaia R., Costa A., Niespolo E.M., Nomade S., Pereira A., Renne P.R.,
410 Hinchliffe A., Mark D.F., Brown R.J., Smith V.C. (2019) Evidence for a large
411 magnitude eruption from Campi Flegrei caldera (Italy) at 29 ka, Geology, doi:
412 10.1130/G45805.1

413 Auker, M.R., Stephen, R., Sparks, J., Siebert, L., Crosweller, H.S., Ewert, J., 2013. A
414 statistical analysis of the global historical volcanic fatalities record Journal of Applied
415 VolcanologySociety and Volcanoes, 2:2

416 Belousov, A., Voight, B., Belousova, M., Muravyev, Y., 2000. Tsunamis generated by
417 underwater volcanic explosions: unique data from 1996 eruption in Karymskoye Lake,
418 Kamchatka, Russia. Pure and Applied Geophysics 157, 1135-1143.

419 Bevilacqua, A., Flandoli, F., Neri, A., Isaia, R., Vitale, S., 2016. Temporal models for the
420 episodic volcanism of Campi Flegrei caldera (Italy) with uncertainty quantification,
421 Journal of Geophysical Research, Solid Earth 121, 7821-7845.

422 Bruno, P.P., 2004. Structure and evolution of the Bay of Pozzuoli (Italy) using marine seismic
423 reflection data: implication for collapse of the Campi Flegrei caldera. Bulletin of
424 Volcanology 66, 342-355.

425 Costa, A., Dell'Erba, F., Di Vito, M.A., Isaia, R., Macedonio, G., Orsi, G., Pfeiffer T., 2009.
426 Tephra fallout hazard assessment at the Campi Flegrei caldera (Italy). Bulletin of
427 Volcanology 71, 259–273.

428 Craig, B.G., 1974. Experimental observations of underwater detonations near the water
429 surface. Los Alamos Scientific Laboratory of the University of California, report LA-
430 5548-MS, UC-34.

D'Argenio, B., Aiello, G., de Alteriis, G., Milia, A., Sacchi, M., Tonielli, R., Angelino, A., Budillon, F., Chiocci, F., Conforti, A., De Lauro, M., Di Martino, G., d'Isanto, C., Esposito, E., Ferraro, L., Iannagi, S., Insinga, D., Iorio, M., Marsella, E., Molisso, F., Morra, V., Passaro, S., Pelosi, N., Porfido, S., Raspini, A., Ruggieri, S., Sarnacchiaro, G., Terranova, C., Vilardo, G., Violante, C., 2004. Digital elevation model of the Naples bay and adjacent areas (Eastern Tyrrhenian sea). In: Pasquaré, G., Venturini, C., Groppelli, G. (eds.) Mapping Geology in Italy. Ed. APAT (Roma), Dipartimento Difesa del Suolo-Servizio Geologico d'Italia (S.EL.CA. Firenze), 21-28.

Davies, G., Griffin, J., Løvholt, F., Glimsdal, S., Harbitz, C.B., Thio, H.K., Lorito, S., Basili, R., Selva, J., Geist, E., Baptista, M.A., 2017. A global probabilistic tsunami hazard assessment from earthquake sources. Geological Society, London, Special Publications, 456, 579.

Deino, A.L., Orsi, G., de Vita, S., Piochi, M., 2004. The age of the Neapolitan Yellow Tuff caldera-forming eruption (Campi Flegrei caldera–Italy) assessed by $^{40}Ar/^{39}Ar$ dating method. Journal of Volcanology and Geothermal Research 133, 157-170.

Di Vito, M.A., Isaia, R., Orsi, G., Southon, J., de Vita, S., D'Antonio, M., Pappalardo, L., Piocchi, M., 1999. Volcanism and deformation since 12,000 years at the Campi Flegrei caldera (Italy). Journal of Volcanology and Geothermal Research 91, 221-246.

Di Vito, A., Acocella, V., Aiello, G., Barra, D., Battaglia, M., Carandente, A., et al. (2016). Magma transfer at Campi Flegrei caldera (Italy) before the 1538 AD eruption. Scientific Reports 6, 32245.

Duffy, D.G., 1992. On the generation of oceanic surface waves by underwater volcanic explosions. Journal of Volcanology and Geothermal Research 50, 323-344.

Egorov, Y., 2007. Tsunami wave generation by the eruption of underwater volcano. Natural Hazards and Earth System Sciences 7, 65-69.

Geist, E.L., Lynett, P.J., 2014. Source processes for the probabilistic assessment of tsunami hazards. Special Issue on Undersea Natural Hazards, Oceanography, 27(2), 86–93.

Glimsdal, S., Løvholt, F., Harbitz, C.B., Romano, F., Lorito, S., Orefice, S., Brizuela, B., Selva, J., Hoechner, A., Volpe, M., Babeyko, A., Tonini, R., Wronna, M., Omira, R.,

460 2019. A new approximate method for quantifying tsunami maximum inundation height
461 probability. Pure and Applied Geophysics, https://doi.org/10.1007/s00024-019-02091-w.

462 Goto, A., Taniguchi, H., Yoshida, M., Ohba, T., Oshima, H., 2001. Effects of explosion energy
463 and depth to the formation of blast wave and crater: field explosion experiment for the
464 understanding of volcanic explosion. Geophysical Research Letters 28, 4287-4290.

465 Grezio, A., Tonini, R., Sandri, L., Pierdominici, S., Selva, J., 2015. A Methodology for a
466 Comprehensive Probabilistic Tsunami Hazard Assessment: Multiple Sources and Short-
467 Term Interactions. Journal of Marine Science and Engineering 3, 23-51.

468 Grezio, A., Babeyko, A., Baptista, M.A., Behrens, J. Costa, A., Davies, G., Geist, E.L.,
469 Glimsdal, S. Gonzàlez, F.I., Griffin, J., Harbitz, C.B., LeVeque, R.J., Lorito, S., Lövholt,
470 F., Omira, R., Mueller, C., Paris, R., Parsons, T., Polet, J., Power, W., Selva, J.,
471 Sörensen, M.B., Thio, H.K., 2017. Probabilistic Tsunami Hazard Analysis: Multiple
472 Sources and Global Applications. Reviews of Geophysics, 55.

473 Guidoboni, E., Ciuccarelli, C., 2011. The Campi Flegrei caldera: historical revision and new
474 data on seismic crises, bradyseisms, the Monte Nuovo eruption and ensuing earthquakes
475 (twelfth century 1582 AD). Bulletin of Volcanology 73, 655–677.

476 Kedrinskii, V.K., 2005. Hydrodynamics of Explosion. Springer, Berlin, Heidelberg.

477 Kirby, J.T., Wei, G., Chen, Q., Kennedy, A.B., Dalrymple, R.A., 1998. FUNWAVE 1.0, Fully
478 nonlinear Boussinesq wave model. Documentation and users manual. Report CACR 98-
479 06, Center for Applied Coastal Research, Department of Civil and Environmental
480 Engineering, University of Delaware.

481 Kokelaar, P., 1986. Magma-water interactions in subaqueous and emergent basaltic
482 volcanism. Bulletin of Volcanology 48, 275-289.

483 Latter, J.N., 1981. Tsunamis of volcanic origin: summary of causes with particular references
484 to Krakatoa, 1883. Bulletin of Volcanology 44, 467-490.

485 Le Méhauté, B.L., 1971. Theory of explosion-generated water waves. In: Chow, V.T. (Ed.)
486 Advances in Hydroscience 7, Academic Press, New York, London, pp. 1-79.

487 Le Méhauté, B.L., Wang, S., 1996. Water waves generated by underwater explosion. Adv. Ser.
488 Ocean Eng., World Sci., Volume10, New Jersey.

489 Lorito, S., Selva, J., Basili, R., Romano, F., Tiberti, M.M., Piatanesi, A., 2015. Probabilistic
490 hazard for seismically induced tsunamis: accuracy and feasibility of inundation maps.
491 *Geophysical Journal International*, 200, 1, 574–588.

492 Maramai, A., Brizuela, B., Graziani, L., 2014. The Euro-Mediterranean Tsunami Catalogue.
493 Annals of Geophysics, 57, 4, S0435.

494 Marti, A., Folch, A., Costa, A., Engwell, A., 2016. Reconstructing the plinian and co-
495 ignimbrite sources of large volcanic eruptions: a novel approach for the Campanian
496 Ignimbrite. Scientific Reports 6, 21220, 1-11.

497 Marzocchi ,W., Sandri, L, Selva, J., 2010. BET_VH: a probabilistic tool for long-time
498 volcanic hazard assessment. Bulletin of Volcanology 72, 705-716.

499 Mirchina, N.R., Pelinovsky, E.N., 1988. Estimation of underwater eruption energy based on
500 tsunami wave data. Natural Hazards 1, 277–283.

501 Morrissey, M., Gisler, G., Weaver, R., Gittings, M., 2010. Numerical model of crater lake
502 eruptions. Bulletin of Volcanology 72, 1169-1178.

503 Newhall, C.G., Hoblitt, R.P., 2002. Constructing event trees for volcanic crises. Bulletin of
504 Volcanology 64, 3-20.

505 Orsi, G., de Vita, S., Di Vito, M.A., 1996. The restless, resurgent Campi Flegrei nested caldera
506 (Italy): constraints on its evolution and configurations. Journal of Volcanology and
507 Geothermal Research 74, 179-214.

508 Orsi, G., Di Vito, M.A., Isaia, R., 2004. Volcanic hazard assessment at the restless Campi
509 Flegrei caldera. Bulletin of Volcanology 66, 514-530.

510 Orsi, G., Di Vito, M.A., Selva, J., Marzocchi, W., 2009. Long-term forecast of eruption style
511 and size at Campi Flegrei caldera (Italy). Earth and Planetary Science Letters 287, 265-
512 276.

513 Paparo, M.A., Tinti, S., 2017. Analysis of Seismic-Driven Instability of Mt. Nuovo in the
514 Ischia Island, Italy. Bulletin of the Seismological Society of America 107, 750-759.

515 Paris, R., 2015. Source mechanisms of volcanic tsunamis. Philosophical Transactions of the
516 Royal Society A 373, 20140380.

517 Paris, R., Ulvrova, M., 2019. Tsunamis generated by subaqueous volcanic explosions in Taal
518 Caldera Lake, Philippines. Bulletin of Volcanology 81, 14.

519 Sandri, L., Costa, A., Selva, J., Tonini, R., Macedonio, G., Folch, A., Sulpizio, R., 2016.
520 Beyond eruptive scenarios: Assessing tephra fallout hazard from Neapolitan volcanoes.
521 Scientific Reports, 6, 24271.

522 Sato, H., Taniguchi, H., 1997. Relationship between crater size and ejecta volume of recent
523 magmatic and phreato-magmatic eruptions: implications for energy partitioning.
524 Geophysical Research Letters 24, 205-208.

525 Selva, J., Costa, A., M.A., Marzocchi, W., Sandri, L., 2010. BET_VH: exploring the influence
526 of natural uncertainties on long-term hazard from tephra fallout at Campi Flegrei (Italy).
527 Bulletin of Volcanology 72, 717-733.

528 Selva, J., Orsi, G., Di Vito, M.A., Marzocchi, W., Sandri, L., 2012a. Probability hazard map
529 for future vent opening at Campi Flegrei caldera, Italy. Bulletin of Volcanology 74, 497-
530 510.

531 Selva, J., Marzocchi, W., Papale, P., Sandri, L., 2012b. Operational eruption forecasting at
532 high-risk volcanoes: the case of Campi Flegrei, Naples. Journal of Applied Volcanology
533 1:5.

534 Selva, J., Costa, A., Sandri, L., Marzocchi, W., 2014. Probabilistic short-term volcanic hazard
535 in phases of unrest: a case study for tephra fallout. Journal of Geophysical Research
536 119(12), 8805-5526.

537 Selva, J., Tonini, R., Molinari, I., Tiberti, M. M., Romano, F., Grezio, A., Melini, D.,
538 Piatanesi, A., Basili, R., Lorito, S., 2016. Quantification of source uncertainties in
539 Seismic Probabilistic Tsunami Hazard Analysis (SPTHA), Geophysical Journal
540 International 205, 1780–1803.

541 Selva, J., Costa, A., De Natale, G., Di Vito, M.A., Isaia, R., Macedonio, G., 2018. Sensitivity
542 test and ensemble hazard assessment for tephra fallout at Campi Flegrei, Italy. Journal
543 of Volcanology and Geothermal Research 351, 1-28.

544 Shi, F., Kirby, J.T., Harris, J.C., Geiman, J.D., Grilli, S.T., 2012. A high-order adaptive time-
545 stepping TVD solver for Boussinesq modeling of breaking waves and coastal

546 inundation. Ocean Modelling 43-44, 36-51.Steinman, L., Spiess, V., Sacchi, M., 2018.
547 Post-collapse evolution of a coastal caldera system: insights from a 3D multichannel
548 seismic survey from the Campi Flegrei caldera (Italy). Journal of Volcanology and
549 Geothermal Research 349, 83-98.

550 Steinmann, L., Spiess, V., & Sacchi, M. 2018. Post-collapse evolution of a coastal caldera
551 system: Insights from a 3D multichannel seismic survey from the Campi Flegrei caldera
552 (Italy). Journal of Volcanology and Geothermal Research, 349, 83-98.

553 Taddeucci, J., Sottili, G., Palladino, D.M., Ventura, G., Scarlato, P., 2010. A note on maar
554 eruption energetics: current models and their applications. Bulletin of Volcanology 72,
555 75-83.

556 Tarquini, S., Isola, I., Favalli, M., Mazzarini, F., Bisson, M., Pareschi, M.T., Boschi, E., 2007.
557 TINITALY/01: a new Triangular Irregular Network of Italy. Annals of Geophysics 50,
558 407-425.

559 Tehranirad, B., Shi, F., Kirby, J.T., Harris, J.C., Grilli, S., 2013. Tsunami benchmark results
560 for fully nonlinear Boussinesq wave model FUNWAVE-TVD, Version 2.1. Research
561 Report N° CACR 13-10, Center for Applied Coastal Research, University of Delaware.

562 Tinti, S., Maramai, A., Graziani, L., 2004. The new catalogue of Italian tsunamis. Nat.
563 Hazards 33, 439-465

564 Tonini, R., Sandri, L., Costa, A., Selva, J., 2015. Brief Communication: The effect of
565 submerged vents on probabilistic hazard assessment for tephra fallout. Natural Hazards
566 and Earth System Science 15, 409-415.

567 Torsvik, T., Paris, R., Didenkulova, I., Pelinovsky, E., Belousov, A., Belousova, M., 2010.
568 Numerical simulation of explosive tsunami wave generation and propagation in
569 Karymskoye Lake, Russia. Natural Hazards and Earth System Sciences 10 (11), 2359-
570 2369.

571 Ulvrova, M., Paris, R., Kelfoun, K., Nomikou, P., 2014. Numerical simulations of tsunami
572 generated by underwater volcanic explosions at Karymskoye Lake (Kamchatka, Russia)
573 and Kolumbo volcano (Aegean Sea, Greece). Natural Hazards and Earth System
574 Sciences 14, 401-412.

575 Ulvrova, M., Paris, R., Nomikou, P., Kelfoun, K., Leibrandt, S., Tappin, D.R., McCoy, F.W.,
576 2016. Source of the tsunami generated by the 1650 AD eruption of Kolumbo submarine
577 volcano (Aegean Sea, Greece). Journal of Volcanology and Geothermal Research 321,
578 125-139.

579 Valentine, G.A., White, J.D.L., Ross, P.S., Amin, J., Taddeucci, J., Sonder, I., Johnson, P.J.,
580 2012. Experimental craters formed by single and multiple buried explosions and
581 implications for volcanic craters with emphasis on maars. Geophysical Research Letters
582 39, L20301.

583 Valentine, G.A., Graettinger, A.H., Macorps, É., Ross, P.S., White, J.D.L., Döhring, E.,
584 Sonder, I., 2015. Experiments with vertically and laterally migrating subsurface
585 explosions with applications to the geology of phreatomagmatic and hydrothermal
586 explosion craters and diatremes. Bulletin of Volcanology 77 (3), 1-17.

587 Volpe, M., Lorito, S., Selva, J., Tonini, R., Romano, F., and Brizuela, B., 2019. From regional
588 to local SPTHA: efficient computation of probabilistic tsunami inundation maps
589 addressing near-field sources. Nat. Hazards Earth Syst. Sci., 19, 455-469.

590 Wohletz, K.H., 1986. Explosive magma-water interactions: thermodynamics, explosion
591 mechanisms, and field studies. Bulletin of Volcanology 48, 245-264.

592

Figure captions

Fig. 1. Location map of the study area. The Pozzuoli Bay corresponds to the southern emerged part of the Campi Flegrei caldera. Bathymetry by D'Argenio et al. (2004).

Fig. 2. A) Physical parameters controlling the initial displacement of the water surface and subsequent tsunami in case of subaqueous volcanic explosion: *E*: explosion energy; *d*: explosion depth; *D*: total water depth around the volcanic cone; *R*: eruptive vent radius; η_0: initial water surface displacement. B) Location of the 17 explosion sites tested for tsunami simulations in the Pozzuoli Bay. C) Craters of past eruptions at Campi Flegrei. The size of the craters (circles) is used to determine the three classes of radii of eruptive vents (modified from Costa et al. (2009). D) Dense Rock Equivalent versus Vent radius showing the relationship between the erupted magma volume and the size of the vents.

Fig. 3. Bayesian Event Tree for Volcanic Hazard (BET_VH) for the Campi Flegrei caldera (modified from Selva et al., 2010) adopted in this study. In light grey, we report the nodes that are not quantified, due to the choice of conditioning the probabilities upon the occurrence of subaqueous explosions.

Fig. 4. Maximum water elevation for explosions at site #1. Three cases of eruptive vent radius are distinguished (200, 650, and 900 m), corresponding to explosion energies of 2.9×10^{14}, 9.8×10^{15}, and 2.6×10^{16} J, respectively (see Table 1). Blue colour corresponds to water displacements inferior to 0.1 cm. Dark blue areas at the edges of the computational domain represent a sponge layer that is prescribed at the grid boundaries in order to dump incoming waves and hence prevent reflections to form at the end walls.

Fig. 5. Maximum wave amplitude recorded at the coast (*Hmax*) as a function of distance along the coastline (starting from the NW) for 3 different explosion sites (#4, #7, and #17). Cities of Pozzuoli, Naples, Torre del Greco, and Castellamare di Stabia are located at distances of 20, 40, 50, and 65 km, respectively.

Fig. 6. Wave heights generated by underwater explosions at site #1 and recorded at the coast at 7 virtual tide gauge stations. Three different values of vent radii (200, 650, and 900 m) are represented, corresponding to different energies of explosion.

Fig. 7. For each individual size class (rows 1 to 3) and their combinations (row 4), we report the conditional mean hazard maps for a probability threshold = 0.05 (maps on the left)

and the conditional hazard curves (mean and 10^{th}-90^{th} percentiles confidence interval) in one point (black square) within the city of Naples (red lines on the right). All hazards are conditional upon submarine explosive eruptions (SEE) of size 1 (top panel), size 2 (second top panel), size 3 (third top panel), and any size (bottom panel). Note that, for sizes 2 and 3 (medium and large vent radia), the hazard curves have probability approaching 1 for relatively small tsunami intensity, meaning that the exceedance of such intensity in that position approaches certainty in case of submarine eruptions of these sizes.

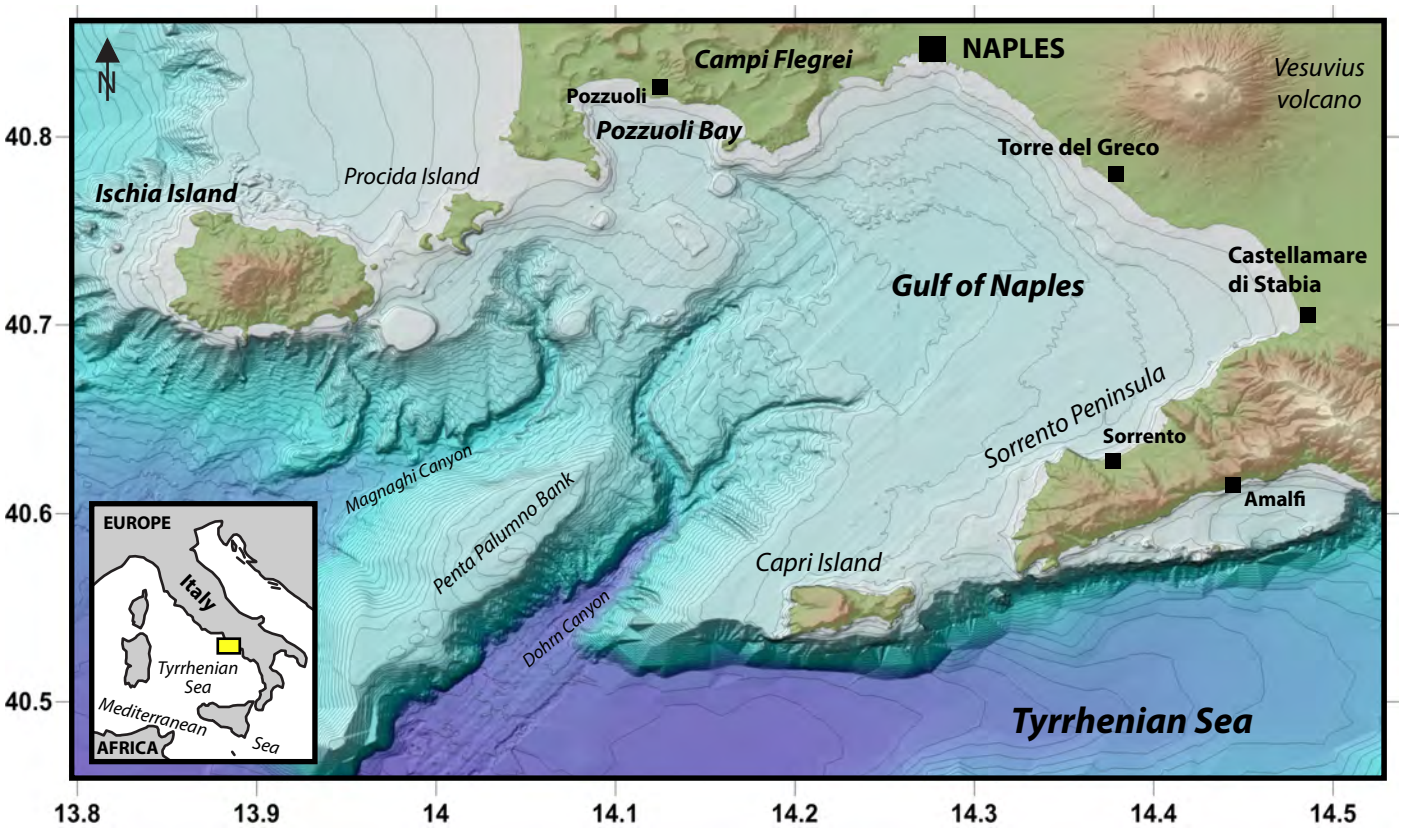
N
NAPLES
Campi Flegrei
Pozzuoli
Pozzuoli Bay
Vesuvius volcano
Torre del Greco
Ischia Island
Procida Island
Gulf of Naples
Castellamare di Stabia
Sorrento Peninsula
Sorrento
Amalfi
Magnaghi Canyon
Penta Palumno Bank
Capri Island
Dohrn Canyon
Tyrrhenian Sea
EUROPE
Italy
Tyrrhenian Sea
Mediterranean Sea
AFRICA
40.8
40.7
40.6
40.5
13.8
13.9
14
14.1
14.2
14.3
14.4
14.5

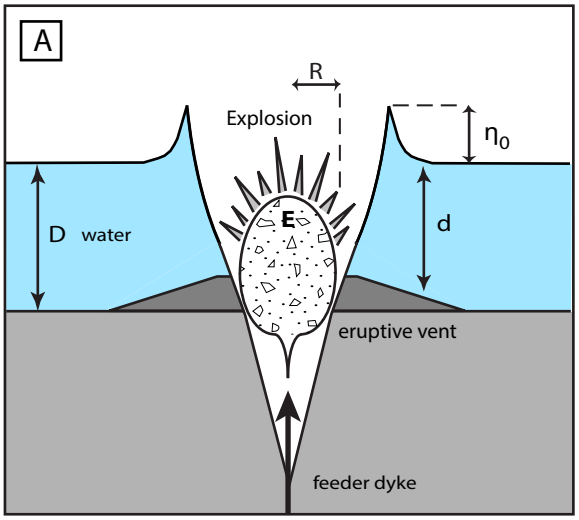
A
R
Explosion
η_0
D water
E
d
eruptive vent
feeder dyke

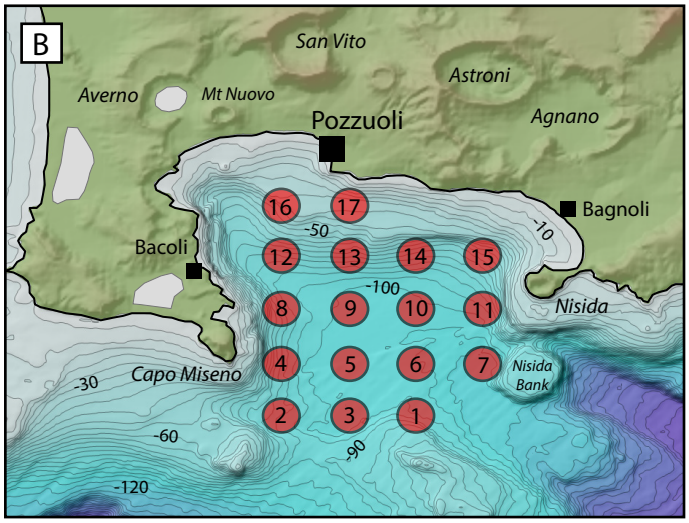
B
San Vito
Astroni
Averno
Mt Nuovo
Pozzuoli
Agnano
Bagnoli
Bacoli
16
17
12
13
14
15
8
9
10
11
4
5
6
7
2
3
1
-10
-50
-100
Nisida
Capo Miseno
Nisida Bank
-30
-60
-90
-120

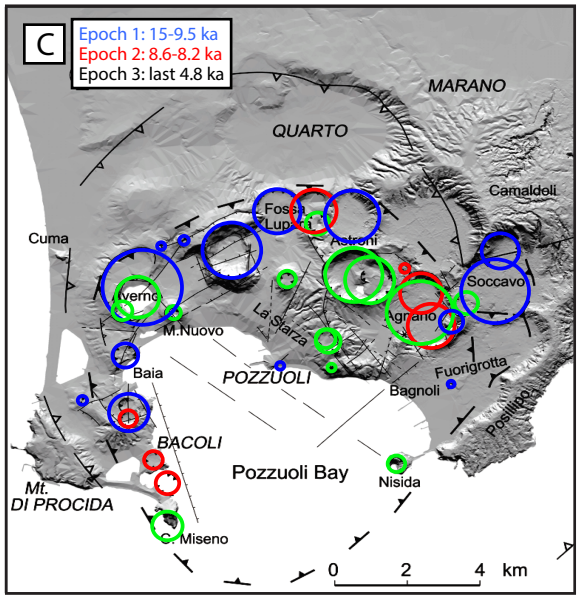
C
Epoch 1: 15-9.5 ka
Epoch 2: 8.6-8.2 ka
Epoch 3: last 4.8 ka
MARANO
QUARTO
Camaldoli
Fossa Lupara
Astroni
Cuma
Averno
Soccavo
Agnano
M.Nuovo
La Starza
Baia
POZZUOLI
Fuorigrotta
Bagnoli
Posillipo
BACOLI
Pozzuoli Bay
Nisida
Mt. DI PROCIDA
C. Miseno
0
2
4
km

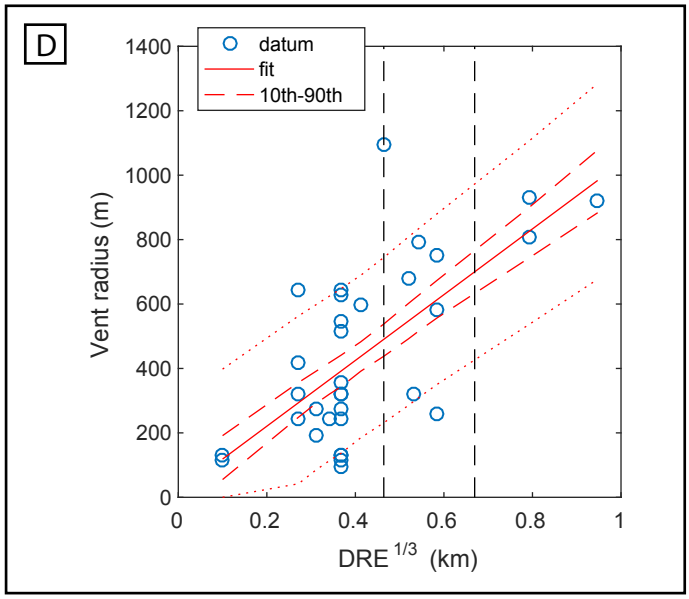
D
datum
fit
10th-90th
Vent radius (m)
1400
1200
1000
800
600
400
200
0
0
0.2
0.4
0.6
0.8
1
DRE 1/3 (km)

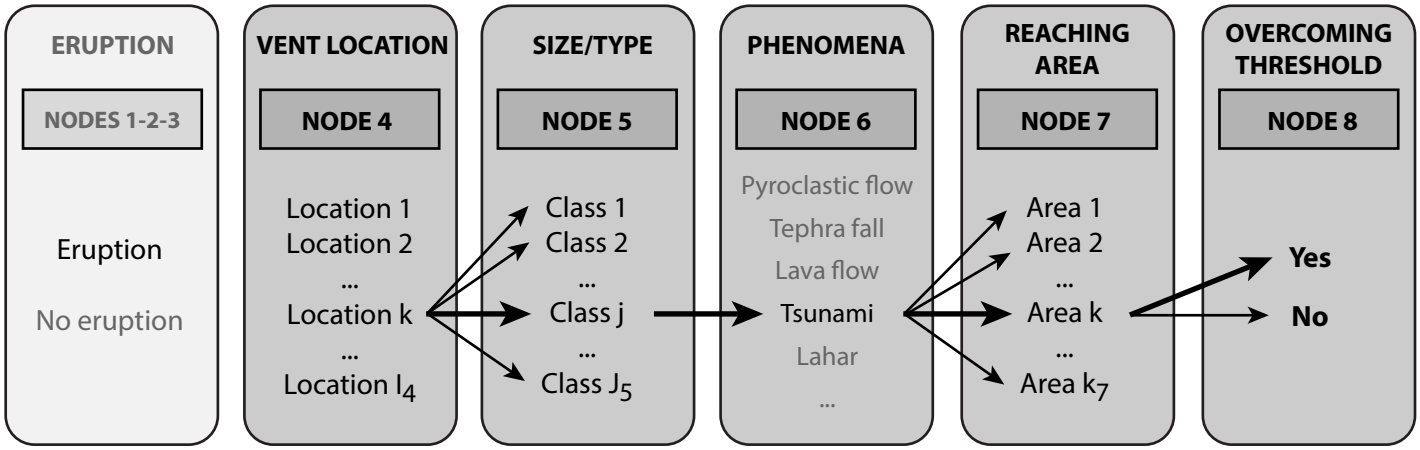
ERUPTION
NODES 1-2-3
Eruption
No eruption
VENT LOCATION
NODE 4
Location 1
Location 2
...
Location k
...
Location l_4
SIZE/TYPE
NODE 5
Class 1
Class 2
...
Class j
...
Class J_5
PHENOMENA
NODE 6
Pyroclastic flow
Tephra fall
Lava flow
Tsunami
Lahar
...
REACHING AREA
NODE 7
Area 1
Area 2
...
Area k
...
Area k_7
OVERCOMING THRESHOLD
NODE 8
Yes
No

Explosion site #1

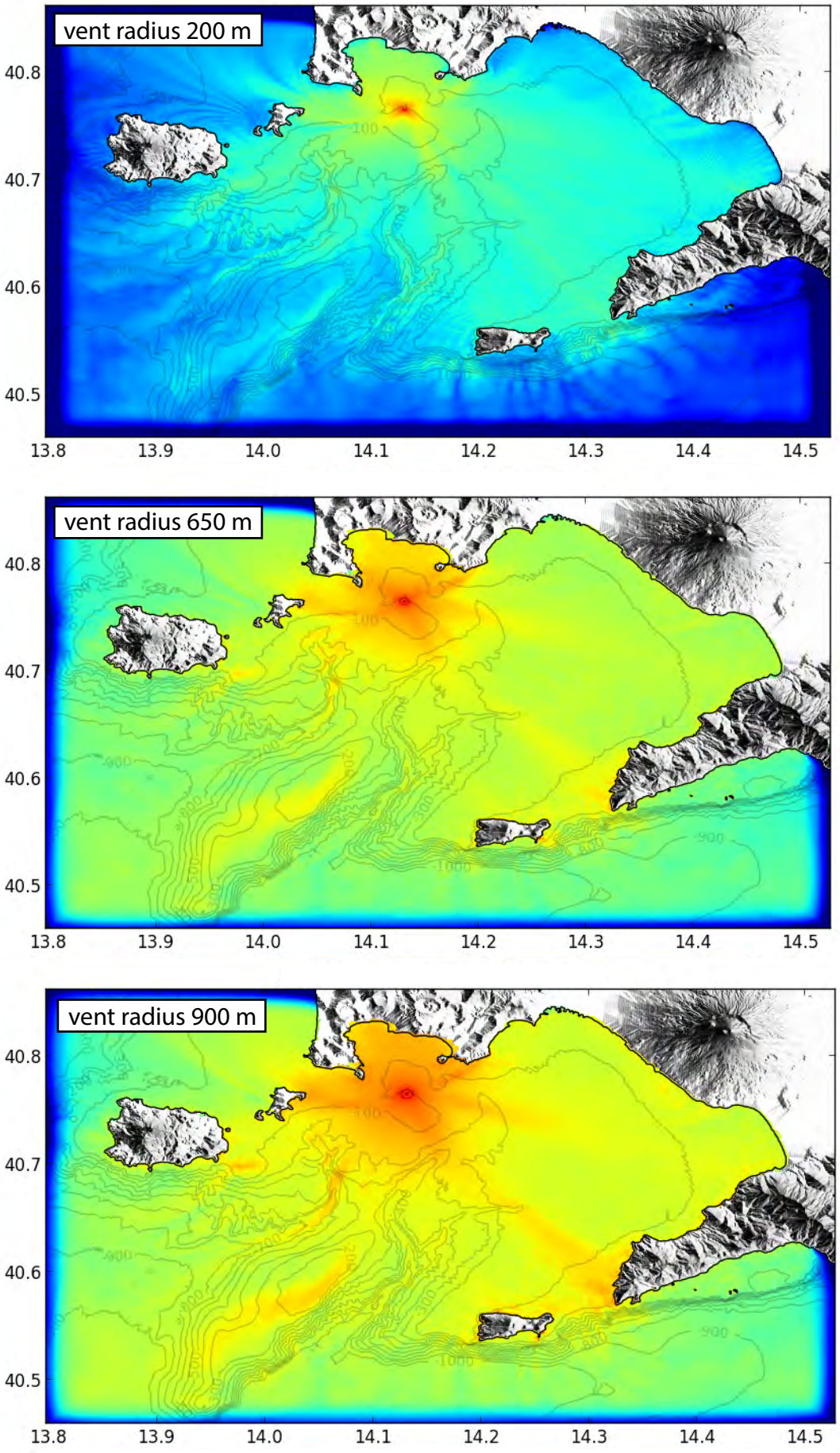

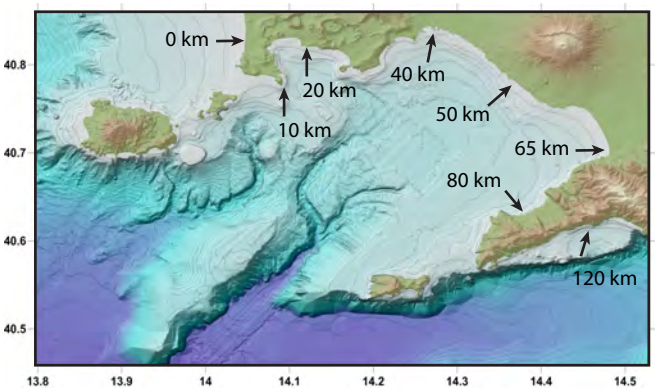

Distance along the coastline (km) from NW to SE

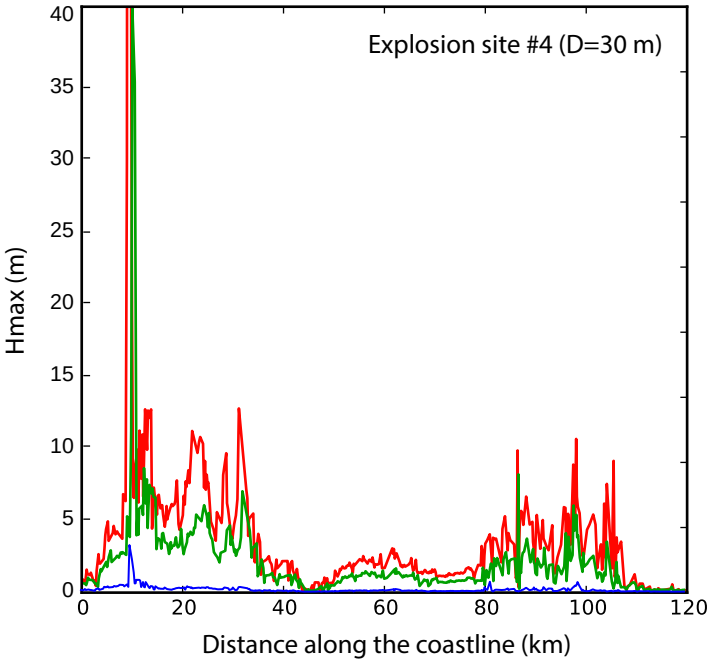

Vent radius (m)
R = 900
R = 650
R = 200

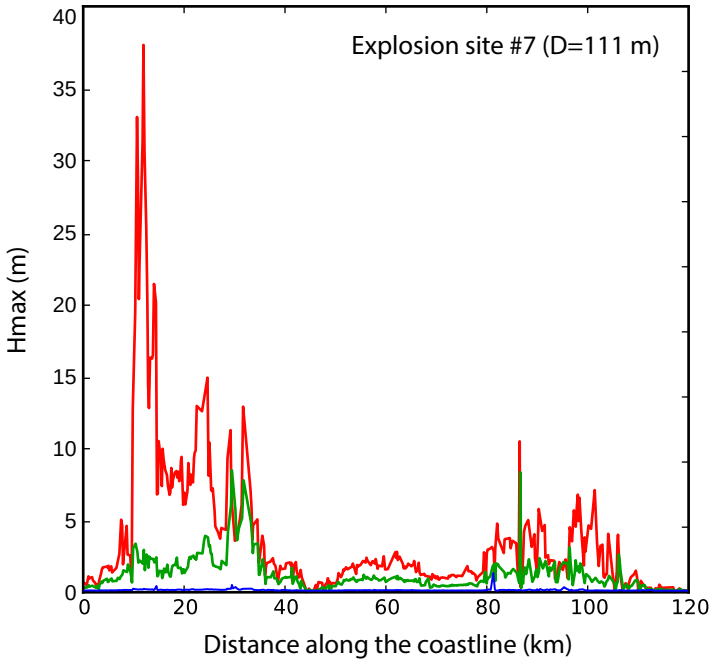

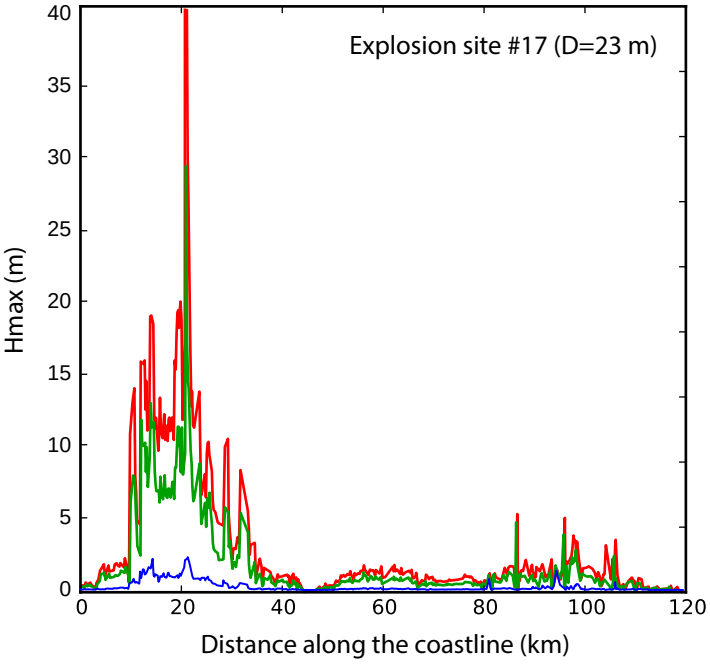

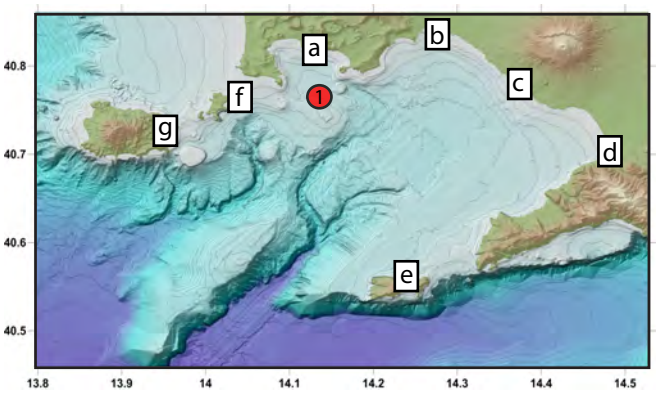

a-Pozzuoli

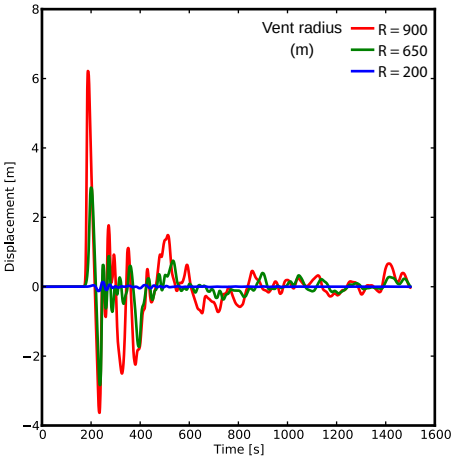

b-Naples

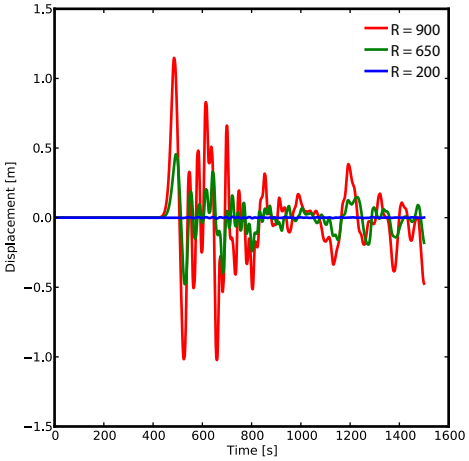

c-Torre del Greco

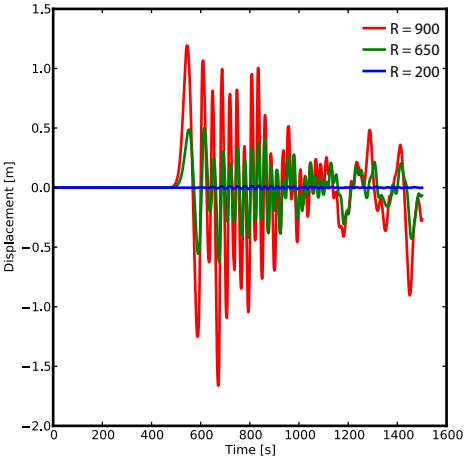

d-Castellamare di Stabia

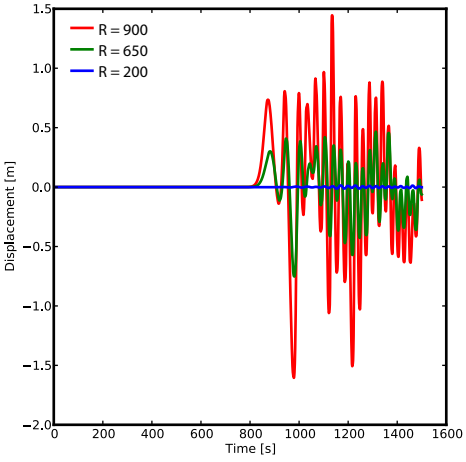

e-Capri

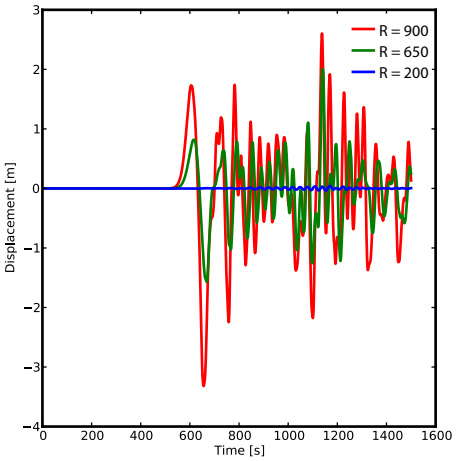

f-Procida

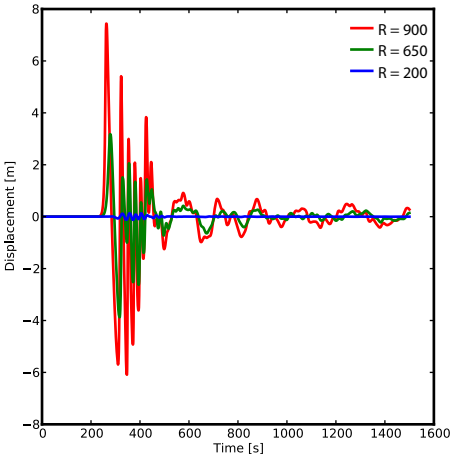

g-Ischia

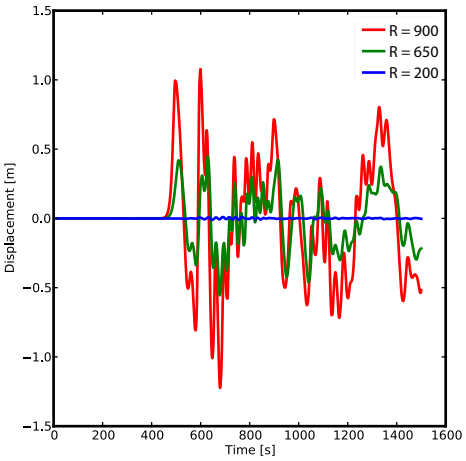

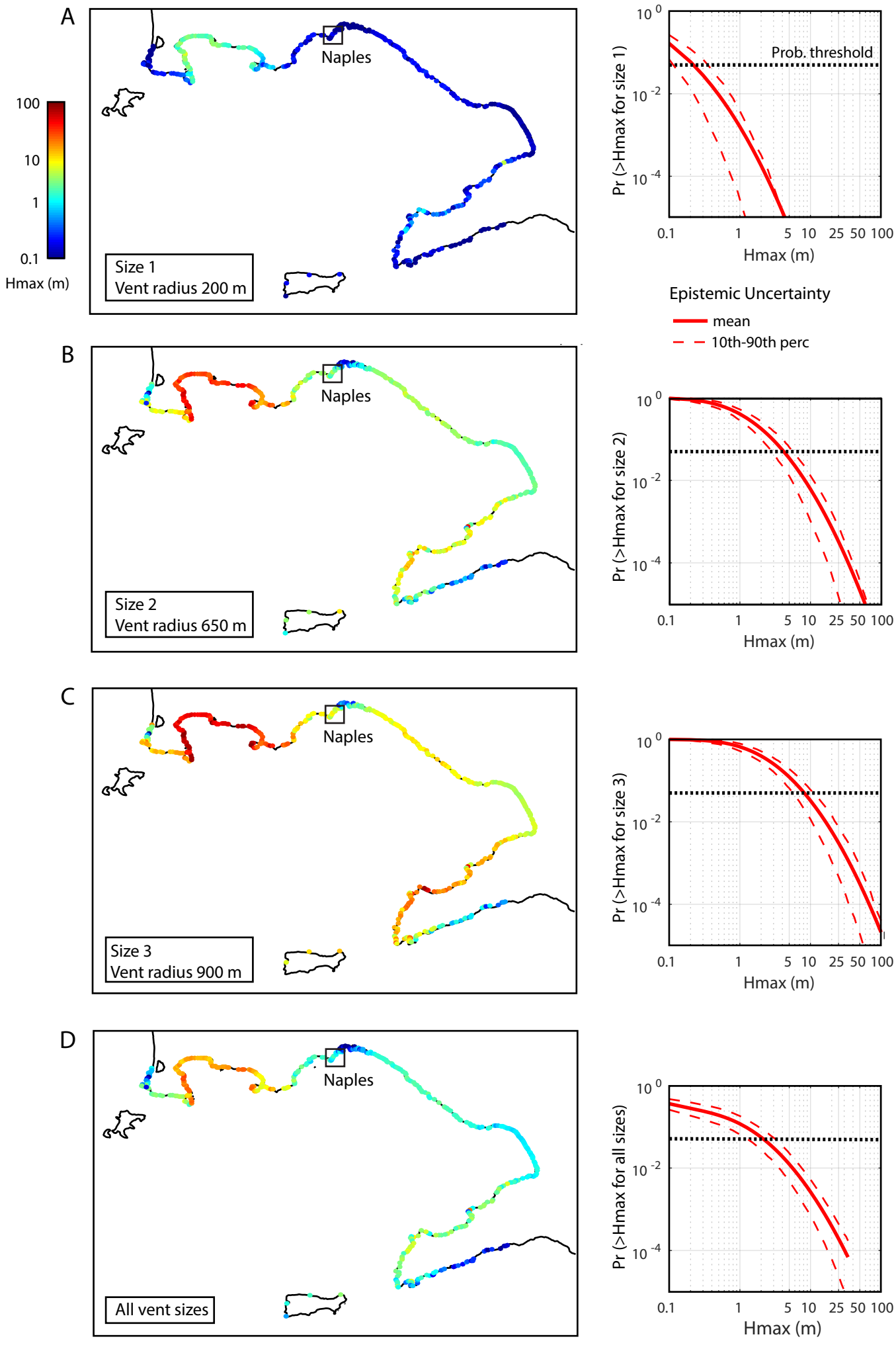
A
B
C
D
100
10
1
0.1
Hmax (m)
Naples
Size 1
Vent radius 200 m
Size 2
Vent radius 650 m
Size 3
Vent radius 900 m
All vent sizes
Prob. threshold
Pr (>Hmax for size 1)
Pr (>Hmax for size 2)
Pr (>Hmax for size 3)
Pr (>Hmax for all sizes)
10 0
10 -2
10 -4
0.1
1
5 10 25 50 100
Hmax (m)
Epistemic Uncertainty
mean
10th-90th perc

Table 1. Scenarios of subaqueous volcanic explosions. d is explosion depth (similar to water depth in this case); R is radius of the eruptive vent; E is explosion energy; η_0 is initial displacement of the water surface.

Explosion site	long (°)	lat (°)	d (m)	R (m)	E (J)	η_0 (m)
1	14.131004	40.76432	93	200	2.90E+14	85
				650	9.80E+15	200
				900	2.60E+16	250
2	14.095464	40.764046	82	200	2.90E+14	85
				650	9.80E+15	200
				900	2.60E+16	250
3	14.113234	40.764184	100	200	2.90E+14	85
				650	9.80E+15	200
				900	2.60E+16	250
4	14.09528	40.777558	28	200	2.90E+14	85
				650	9.80E+15	200
				900	2.60E+16	250
5	14.113054	40.777696	103	200	2.90E+14	85
				650	9.80E+15	200
				900	2.60E+16	250
6	14.130828	40.777831	104	200	2.90E+14	85
				650	9.80E+15	200
				900	2.60E+16	250
7	14.148602	40.777963	111	200	2.90E+14	85
				650	9.80E+15	200
				900	2.60E+16	250
8	14.095097	40.791069	35	200	2.90E+14	85
				650	9.80E+15	200
				900	2.60E+16	250
9	14.112875	40.791207	99	200	2.90E+14	85
				650	9.80E+15	200
				900	2.60E+16	250
10	14.130652	40.791342	101	200	2.90E+14	85
				650	9.80E+15	200
				900	2.60E+16	250
11	14.14843	40.791475	93	200	2.90E+14	85
				650	9.80E+15	200

				900	2.60E+16	250
12	14.094914	40.80458	75	200	2.90E+14	85
				650	9.80E+15	200
				900	2.60E+16	250
13	14.112695	40.804718	63	200	2.90E+14	85
				650	9.80E+15	200
				900	2.60E+16	250
14	14.130476	40.804853	62	200	2.90E+14	85
				650	9.80E+15	200
				900	2.60E+16	250
15	14.148257	40.804986	49	200	2.90E+14	85
				650	9.80E+15	200
				900	2.60E+16	250
16	14.09473	40.818091	37	200	2.90E+14	85
				650	9.80E+15	200
				900	2.60E+16	250
17	14.112515	40.818229	23	200	2.90E+14	85
				650	9.80E+15	200
				900	2.60E+16	250